A Real-Time Non-Implantation Bi-Directional Brain–Computer Interface Solution Without Stimulation Artifacts

Yike Sun, *Graduate Student Member, IEEE*, Anruo Shen, Chenlin Du, Jingnan Sun, Xiaogang Chen, *Member, IEEE*, and Xiaorong Gao, *Member, IEEE*

***Abstract*— The non-implantation bi-directional brain-computer interface (BCI) is a neural interface technology that enables direct two-way communication between the brain and the external world by both "reading" neural signals and "writing" stimulation patterns to the brain. This technology has vast potential applications, such as improving the quality of life for individuals with neurological and mental illnesses and even expanding the boundaries of human capabilities. Nonetheless, non-implantation bi-directional BCIs face challenges in generating real-time feedback and achieving compatibility between stimulation and recording. These issues arise due to the considerable overlap between electrical stimulation frequencies and electrophysiological recording frequencies, as well as the impediment caused by the skull to the interaction of external and internal currents. To address those challenges, this work proposes a novel solution that combines the temporal interference stimulation paradigm and minimally invasive skull modification. A longitudinal animal experiment has preliminarily validated the feasibility of the proposed method. In signal recording experiments, the average impedance of our scheme decreased by 4.59 *k*Ω, about 67%, compared to the conventional technique at 18 points. The peak-to-peak value of the Somatosensory Evoked Potential increased by 8%. Meanwhile, the signal-to-noise ratio of Steady-State Visual Evoked Potential increased by 5.13 *dB*, and its classification accuracy increased by 44%. The maximum bandwidth of the resting state rose by 63%. In electrical stimulation experiments, the signal-to-noise ratio of the low-frequency response evoked by our scheme rose by 8.04 dB, and no stimulation artifacts were generated. The experimental results show that signal quality in acquisition has significantly improved, and frequency-band isolation eliminates stimulation artifacts at the source. The acquisition and stimulation pathways are real-time compatible in this non-implantation bi-directional BCI solution, which can provide technical support and theoretical guidance for creating closed-loop adaptive systems coupled with particular application scenarios in the future.**

***Index Terms*— Brain–computer interface, bi-directional, stimulation artifacts-free, non-implantation, temporal interference.**

Manuscript received 31 May 2023; revised 7 August 2023; accepted 30 August 2023. Date of publication 4 September 2023; date of current version 11 September 2023. This work was supported in part by the National Key Research and Development Program of China under Grant 2022YFC3602803; and in part by the National Natural Science Foundation of China under Grant U2241208, Grant 62171473, and Grant 61671424. *(Corresponding author: Xiaorong Gao.)*

This work involved human subjects or animals in its research. Approval of all ethical and experimental procedures and protocols was granted by the Laboratory Animal Management and Use Committee of the Gateway Medical Innovation Center under IACUC No. BJ2022-05009.

Yike Sun, Anruo Shen, Chenlin Du, Jingnan Sun, and Xiaorong Gao are with the Department of Biomedical Engineering, Tsinghua University, Beijing 100084, China (e-mail: sun.yk.bci@outlook.com; gxr-dea@tsinghua.edu.cn).

Xiaogang Chen is with the Institute of Biomedical Engineering, Chinese Academy of Medical Sciences, Peking Union Medical College, Tianjin 300192, China.

Digital Object Identifier 10.1109/TNSRE.2023.3311750

I. Introduction

BRAIN-COMPUTER interface (BCI) technology is an expanding area of research within the field of neural engineering, defined as a communication system that bypasses the brain's normal output pathways of peripheral nerves and muscles [1]. Recently, the definition of BCI has expanded to encompass applications in medical, educational, and cognitive enhancement domains [2]. Unlike traditional BCIs, which represent the majority of the state-of-the-art, a bi-directional BCI enables complete interaction between the brain and an actuator, thus offering greater clinical and commercial potentials [3]. A bi-directional BCI is a device that capable of reading and writing data from the brain, enabling a complete linkage between the brain and an external device [4]. For instance, a bi-directional BCI can detect an epileptic seizure and stimulate the brain to prevent it [5], or provide tactile feedback to improve the control of a robotic arm [6]. Bi-directional BCIs hold significant promise in medical and cognitive enhancement domains.

The majority of current bi-directional BCI systems rely on implantable devices, such as electrocorticography (ECoG) and deep brain stimulation (DBS), which can acquire high-quality neural signals [7], [8]. However, implantable devices possess several drawbacks that limit their utility and application. First, they have a short lifespan, typically lasting only a few weeks to months [9]. Second, they can cause immune reactions and tissue damage, influencing neural signal stability and reliability [10], [11]. Third, they raise ethical concerns that challenge the research and application of implantable bi-directional BCI technology [12]. Despite recent advances in materials science that have improved the biocompatibility

This work is licensed under a Creative Commons Attribution-NonCommercial-NoDerivatives 4.0 License.
For more information, see https://creativecommons.org/licenses/by-nc-nd/4.0/

of implanted devices, these limitations still exist and require more effective solutions [13]. Consequently, there is a need to develop a high-performance non-implantation bi-directional BCI system, which would significantly enhance the usefulness and applicability of bi-directional BCI technology. In contrast to implantable devices, non-implantation technologies can offer excellent safety and ease of use while reducing patient pain and medical costs.

However, non-implantation bi-directional BCIs face a critical challenge in dealing with the significant interference caused by external stimuli on acquired signals. Conventional electrical stimulation, such as transcranial alternating current stimulation (tACS), generates rapid electric fields with frequencies close to physiological signals around the electrode. Moreover, the magnitude of these fields is usually much larger than the action potential, leading to the masking of crucial physiological information [14]. Furthermore, the presence of stimulus artifacts poses hardware design issues as it can saturate standard neural amplifiers [6]. Many approaches were invented to deal with this issue. These include blanking neural amplifiers during stimulation to prevent saturation, adopting alternating recording and stimulation intervals, recording in between every stimulus, and developing algorithms for extracting signals from mixed data [15]. Although those analytical methods can reduce stimulus artifacts in electroencephalogram (EEG) data, they often come at the cost of reduced decoding information or complete failure to fully restore the original signal [16]. Consequently, non-implantation bi-directional BCIs currently have limited capabilities for real-time feedback, with most studies focusing on post-stimulation effects.

To address the real-time feedback issue of non-implantation bi-directional BCIs, we present a novel solution. We draw inspiration from the temporal interference (TI) electrical stimulation method [17], known for mitigating stimulus interference by utilizing a high-frequency stimulus source to induce a low frequency. However, replicating this TI scheme in a non-implanted setting is challenging due to cranial obstructions [18], [19]. To overcome this cranial interference, we incorporate an ultrasonic drill to enable the interaction of internal and external currents, a technique known as local skull electrophysiological modification (MILEM) [20].

In our evaluation, we focus on testing event-related potentials known for their stable signal quality. Specifically, we examine the Steady-State Visual Evoked Potential (SSVEP) signal in the visual area and the Somatosensory Evoked Potential (SEP) signal in the motor area. Both signals exhibit stable evoked patterns and reproducibility, making them commonly used in electrophysiological research and clinical testing [21], [22]. Furthermore, to mimic the human body environment as closely as possible, we employ sheep as experimental subjects due to their similar skull size and skin thickness to that of humans.

In this study, we present a novel solution that effectively tackles cranial interference using the MILEM technique. Our approach utilizes two high-frequency stimulation sources to induce low-frequency stimulation in vitro, thereby minimizing stimulation artifacts and achieving complete isolation of stimulation and recording frequencies. Consequently, our system enables uninterrupted and simultaneous stimulation and recording, effectively surpassing this limitation. Moreover, our proposed method outperforms existing non-implantable techniques in terms of both recording and stimulation capabilities.

II. Methods

A. The Non-Implantation Bi-Directional BCI Solution

The solution comprises an electrical stimulation part and an electrophysiological recording part, as shown in Fig. 1a. The recording part uses external contact electrodes operating at $\leq 500Hz$. The stimulation part uses two high-frequency sinusoidal stimulation sources with different frequencies and the same type of contact electrodes as the recording part, operating at $\geq 1kHz$. These two parts operate in independent frequency bands and can work simultaneously in vitro. To enhance the access of the stimulation current to the target brain area and improve the recording part's signal quality, we performed local skull modifications by applying ultrasonic vibrations to a needle and disrupting the surrounding bone tissue. The surgical procedure is described in detail below.

The electrical signals from the brain to the scalp have to cross multiple layers of different tissues. Among all the layers, the skull has the lowest electrical conductivity and the most significant impact [18]. As shown in Fig. 1b, cranial modification can partially destroy the cranial tissue. In contrast, the tissue fluid in the organism will rapidly fill the cavity. This effectively reduces the resistivity along the path of ionic currents from the scalp to the brain, thus enhancing the energy of the incoming and outgoing currents. To confirm that our surgical procedure could indeed penetrate the skull, we performed Computed Tomography (CT) imaging. As shown in Fig. 1c and d, the visible length of the needle tip on the multiplanar reconstruction (MPR) image was 1.23 cm. Knowing that the needle tip diameter was 0.5 mm, which was smaller than a pixel (0.7 mm isotropic), and that the overall length of the needle was 1.60 cm, MPR results indicated that the needle tip passed through the skull by at least 0.37 cm. The needle's potential wear during the procedure could lead to a reduction in length, resulting in a slightly smaller actual penetration depth, less than 0.37 cm. No evident bleeding was during the procedure or on CT images.

B. Animal Models

We used 13-month-old male small-tailed sheep as the animal subject in this study. Before the experiment, the sheep were sedated with thioridazine, secured on a surgical table, and intubated. We shaved the hair from the head and neck of the sheep using a razor and hair removal cream and sterilized them with 70% ethanol. We maintained constant and stable anesthesia during the experiments and tests with a mixture of isoflurane and oxygen. The animals' health is continuously monitored by medical equipment. All experimental procedures were approved by the Laboratory Animal Management and Use Committee of the GATEWAY MEDICAL INNOVATION CENTER (IACUC No. BJ2022-05009).

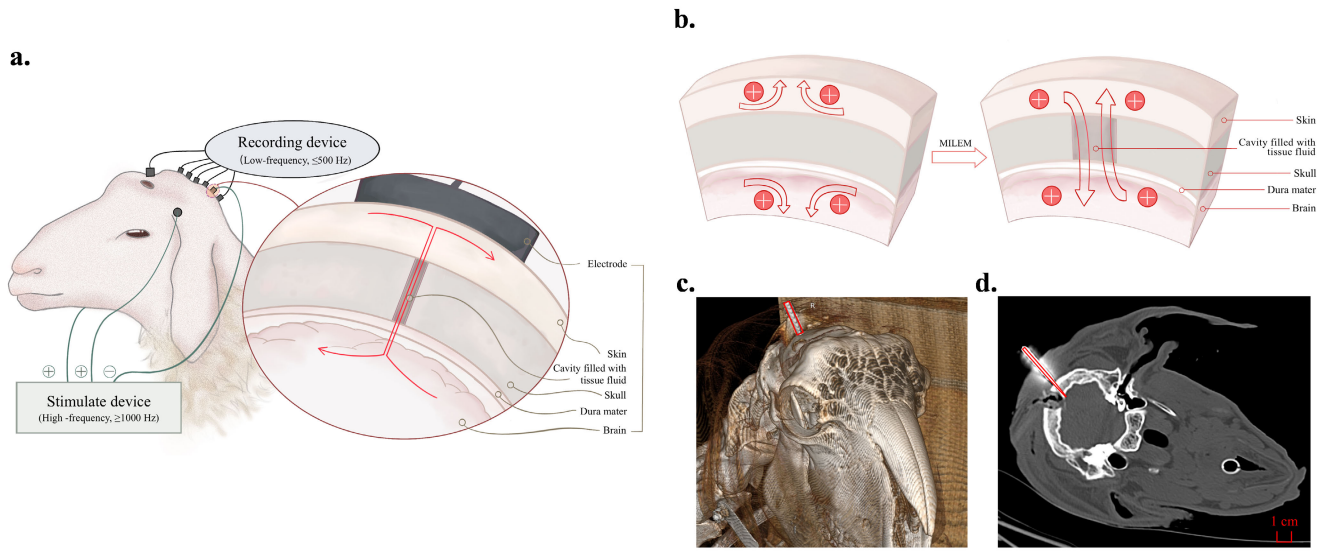

Fig. 1. (a) Schematic diagram of the non-implantation bi-directional BCI solution proposed in this study. The black line with the oval box represents the recording part, which operates at $\leq$ 500Hz, and the green line with the box represents the stimulation part, which operates at $\geq$ 1kHz. The small picture on the right side is a local zoom of the skull modification location in the occipital region. The red arrow represents the ionic current propagation path. (b) Schematic diagram before and after skull modification. The skull modification enhanced the intracranial and extracranial ionic currents. (c) 3D reconstruction of CT images in skull modification. (d) CT image of the cross-section in skull modification. The locations of the stainless-steel nails used in the surgery are outlined with red lines.

C. Minimal-Invasive Skull Modification

We used ultrasound resonance for the modification in the skull modification section. Ultrasound in a specific frequency range can break covalent bonds and vaporize bone tissue without damaging the soft tissues [19]. We made contact with the skull by inserting a stainless-steel needle with a front end that was silicon carbide-plated into the scalp of the target remodeling area. Then The ultrasound was fed into the stainless-steel needle through a piezoelectric ceramic transducer with an output frequency range of $28,000Hz$ to $35,000Hz$ and an output power of $50W$. The operation duration was controlled within $30s$ without damaging the dura mater.

We measured the change in the electrical impedance value of current propagation channel before and after the modification using an LCR700 precision digital bridge (test frequency: $1000Hz$, test AC signal: 0.63 $Vrms$, accuracy: $\pm[0.3\% + 1]$) produced by SANWA. We selected the parallel mode to measure the equivalent resistor value and connected the positive and negative electrodes of the digital bridge to two patch-type Ag/AgCl electrodes. We individually fixed the negative electrode above the sheep's right temporal region, moved the positive electrode onto the 18 points in the parietal and occipital regions, and recorded the readings.

D. Methods for Generating Evoked Potentials

In order to quantitatively assess the degree of improvement of electrophysiological recordings with our proposed protocol, we chose two evoked potentials, SSVEP and SEP, for comparison.

To induce SSVEP response. We presented periodic visual stimuli on a liquid crystal display (model: BENQ XL2720-B, size: 27 inches, resolution: 1920×1080 pixels, refresh rate: $144Hz$) using the sampled sinusoidal stimulation method [24], [25]. We tested nine stimulation frequencies while avoiding breach rhythm [26] [$11Hz$, $12Hz$, $13Hz$, $14Hz$, $15Hz$, $16Hz$, $17Hz$, $18Hz$, $19Hz$, $20Hz$]. The stimulation form was:

$$B(f,i) = Round(255 * 0.5 * \{1 + sin[2\pi f \frac{i}{RefreshRate}]\}) \quad (1)$$

where B represents the display's brightness, an integer between 0 and 255. f represents the stimulation frequency. i represents the serial number of each frame in the stimulus sequence. The round represents the rounding operation. $RefreshRate$ represents the screen's refresh rate, which was 144 in this study. This simulation scheme uses the impulse sequence with a time interval of $1/RefreshRate$ to perform a zero-order sampling hold operation on the sinusoidal signal.

We wrote the stimulation and interface program using MATLAB R2022a and Psychtoolbox-3 [27]. We displayed each frequency stimulus on the full screen (1920×1080 pixels). A single stimulus trial lasted 10 s, with a $5s$ break between trials. We presented five trials for each stimulus frequency and randomly generated the presentation sequence of the trials by the computer. An event trigger was transmitted to the amplifier at the beginning of each stimulation to ease subsequent data analysis. We set the distance between the screen and the sheep to exactly $20cm$ in the front. We fixed the eyelids of the sheep open to ensure watching while using saline to keep the eyes wet.

To generate SEP, we stimulated the median nerve of the right front leg of the sheep using a square wave electrical stimulation instrument produced by NEUSEN. We used two silver microneedles with a diameter of $350\mu m$ as the stimulation electrodes and separated them by $5cm$. The square wave signal generated by the instrument had a rising and

falling period of $5\mu s$ each. The monophasic stimulation pulse width was $200\mu s$, the frequency was 5 Hz, and the current value was $15mA$. We applied electrical stimulation for $200s$ in each experiment, and $500ms$ for each trial, with a total of 1000 trials. We observed apparent muscle twitches in the right forelimb of the sheep during the electrical stimulation.

E. Electrophysiological Recording and Electrical Stimulation In Vitro

This experiment used 20 patch-type Ag/AgCl electrodes (18 for signal leads, one for REF lead, and one for GROUND lead). For signal recording, we used the NEUSEN W wireless amplifier (sampling rate: $1kHz$, standard mode rejection ratio: $120dB$, AD conversion bit: $24bit$, input noise: $\leq 0.4\ uVrms$) produced by NEURACLE company. We placed the reference electrode on the right side of the forehead and the ground electrode on the left side and subsequently divided the signal leads into two groups of nine, each 3×3 array in the occipital and parietal regions. Adjacent electrodes were separated by $3cm$. We controlled the contact impedance of each signal lead within $10k\Omega$ during the acquisition process. The electrode locations were selected based on a specific criterion. As depicted in Fig. 2a, the electrodes were positioned along the median axis, aligning with the line between the occipital bone and the nasal bone. The spacing between each electrode was set at 2 cm.

In Vitro Electrical Stimulation, we used $10Hz$, $20Hz$, and $40Hz$ as the different frequencies for the stimulation. According to Grossman et al. a carrier of $1kHz$ and above is necessary to ensure that the nerve cells are responding following the difference frequency rather than the carrier [17]. Therefore we used $1kHz$ as the carrier wave. Using an external high-power resistance, we converted a dual-channel ATG-2082 power signal source (AIGTEK; voltage: $400Vp$, current: $0to40\ mAp$, bandwidth: $DCto200kHz$, slew rate $\geq 356V/\mu s$) into a dual-channel current source with a synchronous output of $1(\pm0.12)mA$ sinusoidal signal. We placed the positive stimuli in the bilateral temporal regions and the two co-negative stimuli in the center of the occipital region. The stimulating electrodes were four Ag/AgCl electrodes. It is worth noting that while our technical approach drew inspiration from TI [17], we distinguish our work from the original by exclusively conducting the stimulation process in vitro. The three stimulation frequency combinations we applied were: [1 kHz, 1.01 kHz], [1 kHz, 1.02 kHz], and [1 kHz, 1.04 kHz]. Each stimulation lasted $10s$.

F. Data Preprocessing and Analysis

We divided the data into segments based on the recorded trigger for the SSVEP analysis. The data segments with the same stimulation frequency were averaged. We further filtered the data using an IIR filter with $5Hz$ to $20Hz$ passbands and downsampled the filtered data to $250Hz$. For the SEP analysis, we filtered the data using a high-pass IIR elliptic filter with a $50Hz$ cut-off frequency [28], and averaged the recorded 1000 trials. For the resting state data, analysis was done by removing the DC and power frequency components using a comb-shaped IIR filter with a quality factor of 40. We then applied a high-pass FIR filter with an $8Hz$ cut-off frequency to the recorded signal. Any leads with obvious abnormal frequencies were substituted in the subsequent analysis by the mean of the adjacent leads. We implemented all filtering operations using the $filtfilt()$ function in MATLAB R2022a.

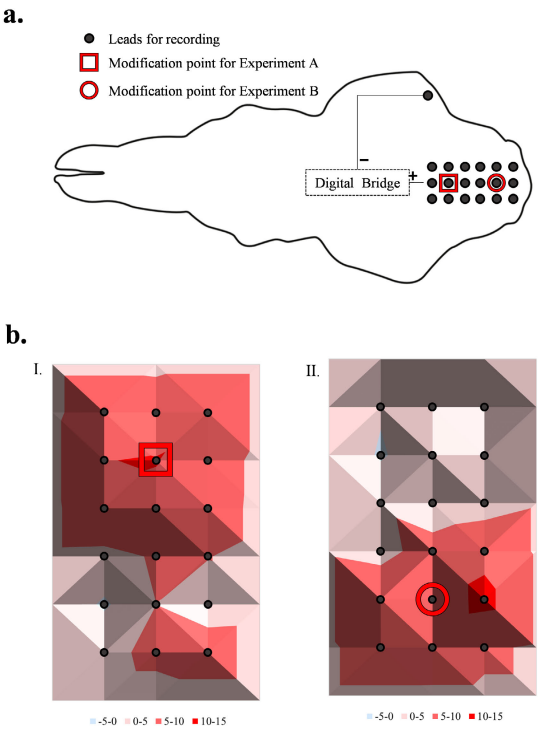

Fig. 2. Electrical impedance test results. (a) Point location diagram of the electrical impedance test experiment. The black origin represents the location of the 18 test points, which are arranged in a 3×6 array in the parietal and occipital regions. The red box marks the modified point location of experiment A, and the red circle box marks the modified point location of experiment B. The negative terminal of the digital bridge was fixed in the right temporal region of the sheep, and the values of each test site were obtained by sequential traversal. (b) Topographic maps of the electrical impedance decrease measured by the digital bridge, which is the pre-modification resistance value minus the post-modification resistance value in $k\Omega$. The higher the decrease, the more the spot color is skewed toward red. The test frequency of the digital bridge was $100Hz$, and the test mode was a parallel connection. (b) I. Impedance decreased values before and after the modification of the parietal region. The location of this modification point was the center of the parietal area, marked with a red box in the figure. (b) II. Impedance decreases values before and after the modification of the occipital region. The location of this modification point was the center of the occipital area, marked with a red circle box in the figure.

In the SSVEP classification task, we used the FBCCA algorithm [29]. The method is divided into three main steps. The first step passes the preprocessed data through each of the five filters ([6 Hz, $90Hz$], [14 Hz, $90Hz$], [22 Hz, $90Hz$], [30 Hz, $90Hz$], [38 Hz, $90Hz$]) to get five data matrices. In the second step, five ρ-values for each of the ten stimulus targets are obtained using sine and cosine templates for each stimulus frequency to calculate the CCA correlation. In the third step, squares of the five ρ-values are summed according to their weights. The highest result among the ten stimulus targets is selected as the predicted frequency.

In data analysis, we used broadband signal-to-noise ratio (SNR) [30], [31] as a metric to reflect the signal quality in

physiological signal processing comprehensively. The main idea was to treat the energy component of the target frequency as a signal and the energy components of all other frequencies as noise. We calculated all SNR indicators in this paper according to broadband SNR. Its calculation formula was:

$$SNR = 10 * \log_{10}[\frac{N(f_{Target})}{\sum_{f=f_l}^{f_h} N(f) - N(f_{Target})}] \quad (2)$$

where SNR represents the value of broadband SNR. f_{Target} is the target signal frequency, the stimulation frequency in SSVEP analysis, and the difference frequency in electrical stimulation analysis. $N(f)$ is the energy component at frequency f. f_h and f_l are the upper and lower limits of the frequency band.

To determine the PSD and maximum bandwidth of the resting state signal, we first applied the Welch technique for spectral estimation. A Hamming window was used as a window function with 50% overlap. The trend line was drawn using the moving average approach with a sliding window length of 30 points to make it easier to understand the PSD map before and after the skull modification. Following several earlier research, we utilized a statistical test and estimated the maximum signal bandwidth before and after the modification [32, 20]. We hypothesized that the signal obtained from in vitro measurements at approximately $100Hz$ encompasses a significant amount of ambient noise components, outweighing the effective information. Therefore, we used the $85Hz$ to $95Hz$ band as the noise floor, as it was the highest $10Hz$ band within $100Hz$ that avoided both the powerline frequency and its harmonics. We performed a paired t-test between the energy value array of any $10Hz$ band and that of the noise floor, and if the band's significance level was below 0.01, we deemed that the band contained effective information. We started from $0Hz$ and traversed through all $10Hz$ bands until the significance level was higher than 0.01. Then we regarded the starting frequency of this band as the highest valid frequency.

III. Results

A. Electrical Impedance

To investigate the impact of skull modification on the reduction of electrical resistivity, we conducted animal experiments to record changes in resistance values before and after modification. The recording sites were identified as shown in Fig. 2a. The instrumentation and experimental parameters used in the tests are described in the Methods section. Two sets of experiments targeting different brain regions were conducted in parallel to allow for a comprehensive comparison. In experiment A, we performed a skull modification at the central point of the parietal region, indicated by the red box in Fig. 2a. Following the modification, we observed a significant decrease in the electrical impedance values recorded at a total of 18 test sites in the parietal and occipital regions ($M = 1.94\ k\Omega, SD = 1.05$) as compared to the values prior to modification ($M = 8.4\ k\Omega, SD = 2.37$), $t(17) = 9.95$, $p = .000000017 \ll .01$. In experiment B, we conducted a skull modification at the center of the occipital region, as indicated by the red circular box in Fig. 2a. Similarly, a significant decrease emerged in resistance values recorded at the 18 tested sites after the modification ($M = 2.28\ k\Omega, SD = 0.83$) compared to those prior to the modification ($M = 6.87\ k\Omega, SD = 3.37$), $t(17) = 6.04$, $p = .00000013 \ll .01$. These results provide solid evidence to support the significance and validity of skull modification as a strategy to reduce electrical resistance values. The experimental findings reveal significant lateralization in the spatial distribution of the impedance reduction resulting from skull modification. To illustrate this effect, we plotted the topographic distribution of the electrical impedance reduction values (pre-modification electrical impedance values minus post-modification electrical impedance values in $k\Omega$) induced by skull modification, as shown in Fig. 2b. Specifically, Fig. 2b I. depicts the results of experiment A, with the modification site located in the parietal region, while Fig. 2b II. illustrates the results of experiment B, with the modification site located in the occipital area. Markers indicate the modification sites in both experiments in the figures. Notably, the electrical impedance reduction due to modification was more pronounced near the modification site, as demonstrated by the topographic maps.

B. Evoked Potential Recording for BCI

After demonstrating that skull modification reduces electrical impedance, this work further assessed its specific effects on electrophysiological recordings. In the two experiments mentioned in the Electrical Impedance section, we also performed evoked potential recordings before and after the modification. In the parietal region of experiment A, an electrical stimulus was given at the median nerve for recording the somatosensory evoked potential (SEP) before and after the modification. In experiment B for the occipital region, we recorded the SSVEP before and after the modification using cyclic visual stimulation in different frequencies. Fig. 3a. shows the locations of the recording electrodes and the modified sites. Fig. 3b. shows the SEP recorded at the center of the parietal region in experiment A (after averaging 1000 trials). A clear N20 and P23 component is visible, and the peak amplitude after the modification ($8.01\mu V$) is about 8% higher than before ($8.68\mu V$). In experiment B, Fig. 3C. and 3D. show the time-frequency representations of the signals recorded at the central occipital region under SSVEP stimulation at $11Hz$ before and after the modification, respectively, along with the spectrograms (the results of five 10-second trials averaged by superposition). The improvement of the SSVEP signal quality by the skull modification is evident in both time and frequency domains. The mean signal-to-noise ratio (SNR) of the SSVEP at the occipital region at each stimulation frequency after skull modification ($M = -10.47\ dB, SD = 1.74$) was significantly higher than the one before modification ($M = -15.6\ dB, SD = 2.78$), $t(9) = -6.88$, $p = .000072 \ll .01$, as shown in Fig. 3e. The average increase was about $5.13\ dB$. To verify the effect of signal boosting on the performance of the BCI, we used the filter bank canonical correlation analysis (FBCCA) algorithm to classify the acquired data for SSVEP stimulation frequency prediction. Fig. 3f. and Fig. 3g. show the confusion matrix and the accuracy of the classification results, respectively. Fig. 3f I. shows the classification results

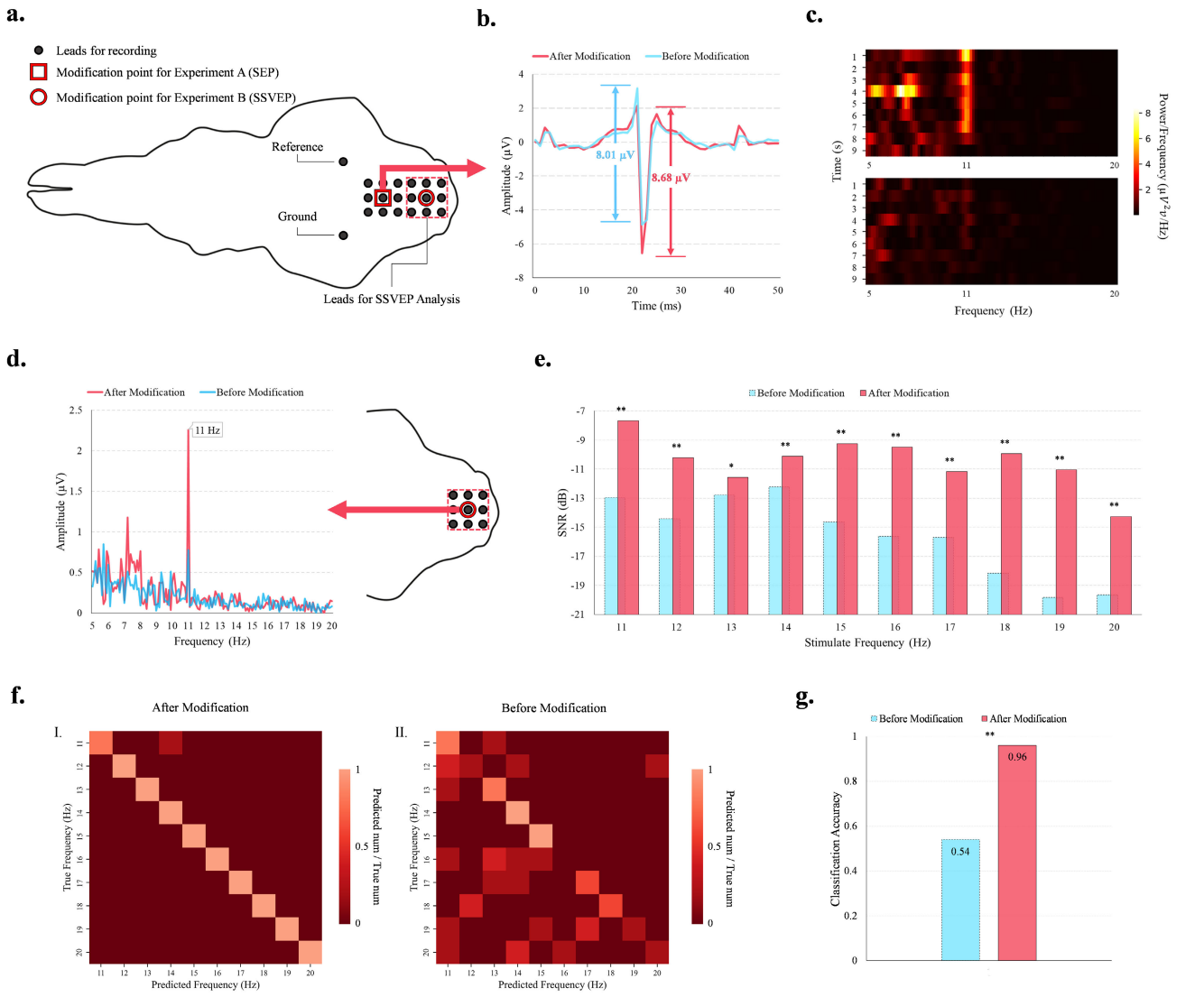

Fig. 3. Electrophysiological recordings. (a) Recording sites. Eighteen recording electrodes are arranged in a 3×6 pattern in the parietal and occipital regions of the sheep. The red boxes and circles mark the locations of the modification sites in experiments A and B, respectively. (b) SEP was recorded after averaging 1000 trials. The red and blue curves show the results after and before cranial modification. The peak-to-peak amplitudes after and before the modification are also marked, with values of 8.68μV and 8.01μV, respectively. (c) Time-frequency representation of the signal recorded at the central dotted lead of the occipital region under SSVEP stimulation at 11Hz. The upper and lower panels show the results after and before the modification. The darker red color indicates low energy, and the more yellow color indicates high energy. (d) The amplitude-frequency representation of the signal recorded at the central point lead of the occipital region. The red and blue lines show the results after and before the modification. (e) the Broadband signal-to-noise ratio of the SSVEP recorded at each stimulation frequency. The result is the average of the 9-lead SNR across the occipital region. The red and blue bars show the results after and before modification. (f) I. is the confusion matrix of SSVEP classification prediction results after the modification, and II. is the confusion matrix before the modification. (g) red represents the SSVEP classification accuracy after the modification, and blue represents the accuracy before the modification.

after the modification and Fig. 3f II. shows the results before the classification. It can be seen that the skull modification has an obvious improvement in the classification performance of the BCI. The accuracy of SSVEP classification after the modification ($M = 0.98, SD = 0.06$) was significantly higher than that before the modification ($M = 0.54, SD = 0.37$), $t(9) = -3.6$, $p = .0057 < .01$, as shown in Fig. 3g.

C. Resting-State Frequency Band Enhancement

We analyzed the resting-state data before and after the modification to measure the change in the maximum effective bandwidth of the electrophysiological recording section. We first calculated the average PSD maps of the nine leads in the parietal region of experiment A and the nine leads in the occipital region of experiment B. Then we performed a statistical analysis to determine the maximum effective bandwidth. Fig. 4a. shows that for experiment A, the mean maximum effective bandwidth of the parietal region 9-lead after cranial modification ($M = 50.7\ Hz, SD = 16.85$) was significantly higher than before modification ($M = 38.2\ Hz, SD = 4.47$), $t(8) = -2.38$, $p = .044 < .05$. The average increase was about 33%. Fig. 4b. shows that for experiment B, the maximum effective bandwidth of the occipital region 9-lead after cranial modification ($M = 62.4\ Hz, SD = 14.54$)

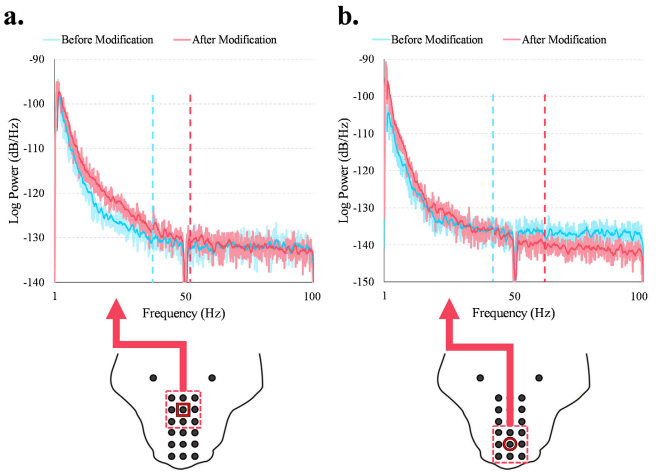

Fig. 4. Resting-state electrophysiological recordings. (a) Average PSD maps in the parietal region before and after the modification. (b) Average PSD maps in the occipital region before and after the modification. The locations of the leads used for the analysis and the corresponding modification sites are indicated below. The light red and blue curves show the results after and before the modification. The red and blue lines show the moving averages of the PSD plots after and before the modification, respectively. The red and blue vertical dashed lines indicate the maximum effective bandwidth after and before the modification. The energy drops around 0*Hz*, 50*Hz*, and 100*Hz* due to the industrial frequency removal operation.

was also significantly higher than before modification ($M = 38.24\ Hz, SD = 1.7$), $t(8) = -4.9$, $p = .0012 < .01$. The average increase was about 63%. The occipital region's results may be better due to its greater distance from the Ground and Reference lead. These results suggest that skull modification enhances the effective bandwidth of the electrophysiological recording section in the resting state. This phenomenon may indicate that as the local electric impedance of the skull decreases, more information can be transmitted from the brain to the scalp. It suggests more possibilities for non-implantation BCIs.

D. Bi-Directional in Vitro Implementation of AC Stimulation and Recording

Fig. 5a. shows the distribution of electrical stimulation and electrophysiological recording points. Because the frequency range used in our stimulation protocol was isolated from the frequency range of the electrophysiological recordings, we could record the effects of electrical stimulation in real-time. We performed three-point skull modifications to ensure the stimulation current could enter the brain and activate neurons. We tested three different stimulation combinations, which are [$1kHz$&$1.01\ kHz$, $1kHz$&$1.02\ kHz$, $1kHz$&$1.04\ kHz$]. The specific parameters and technical details of the electrical stimulation are given in Methods. We calculated the SNR before and after the modification to quantify the enhancement of the electrical stimulation effect by the cranial modification. Fig. 5b. shows that the SNR of the frequency component at the differential frequency of two stimulus sources, Δf (for three combinations: $10Hz$, $20Hz$, $40Hz$), was significantly higher after skull modification ($M = -10.48\ dB, SD = 0.33$) than before modification ($M = -18.52\ dB, SD = 1.36$), $t(3) = -13.41$, $p = .005 < .01$. The average increase was about 8.04 dB. Fig. 5c. shows the topographic distribution of the SNR increase at the Δf frequency component for the 18 leads. The values refer to the SNR differences before and after the modification in dB. This figure implies that the electric field distribution was more focused and had a higher spatial resolution after the skull modification. The amplitudes of the Δf frequency components we recorded in our experiments were on the order of microvolts. As shown in Fig. 5d, our electrical stimulation was on the order of millivolts, indicating that our stimulation protocol successfully induced clustered oscillations of neurons. Moreover, Fig. 5d. also shows that the amplitude of the Δf frequency component before skull modification did not exhibit a significant peak. This experimental observation suggests that the in vitro realization of the TI stimulation may not be achievable directly without skull modification. Thus, we posit that reducing the electrical impedance of the skull is imperative for successful TI stimulation in vitro. In other words, the induction of Δf through skull modification can be viewed as a transition "from absence to presence" rather than a mere enhancement.

Finally, in order to illustrate the superiority of the TI stimulation scheme, we conducted an experiment wherein both stimulation sources were directly stimulated at a frequency of Δf for low-frequency stimulation, and the resulting signals were recorded. Fig. 5e presents a comparison of the obtained results for the case when Δf is set to $10Hz$. The figure clearly indicates that direct low-frequency stimulation leads to significant stimulation artifacts, completely overshadowing the electrical signals generated by neural activity, with their amplitude surpassing the neural signals by several orders of magnitude. In contrast, the TI stimulation scheme, depicted in red in Fig. 5e, effectively circumvents the interference caused by stimulation artifacts, enabling direct recording of the neural signals.

IV. Discussion

This paper presents an innovative real-time, non-implantation, bi-directional BCI solution that enables simultaneous high-quality brain activity recording and precise modulation. This advancement offers new tools and methodologies for brain science and brain-computer interaction. Our approach relies on local skull electrical modification, achieved through the use of ultrasound resonance to evaporate specific skull tissue, thus reducing the electrical impedance of the targeted skull region. As a result, this technique mitigates the skull's blocking effect on electrical signals, enabling more accurate and sensitive measurement of electrophysiological signals through external electrodes. This represents a substantial improvement over conventional EEG techniques.

Furthermore, we leverage the reduced resistance in the current propagation path resulting from skull modification to design an in vitro TI scheme. This scheme involves applying two high-frequency AC currents with electrodes to induce low-frequency responses in targeted brain areas. Importantly, the stimulation frequency employed in this scheme does not

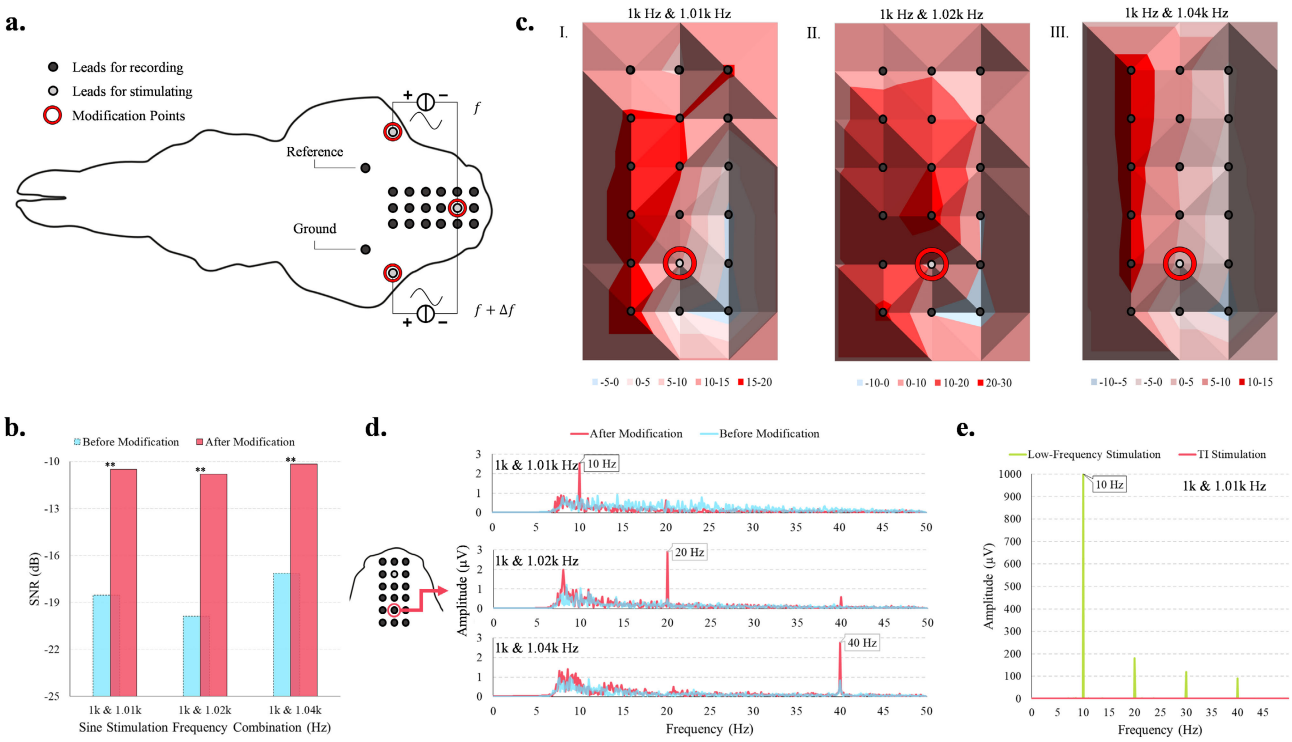

Fig. 5. Results of simultaneous electrical stimulation and electrophysiological recordings. (a) Distribution of leads for electrical stimulation and electrophysiological recording. The grey leads are used for electrical stimulation, and the black leads are used for electrophysiological recordings. The skull modification sites are marked with red circles. A sinusoidal cross-current stimulus with frequency f was applied between the right temporal and occipital regions for electrical stimulation. In contrast, a sinusoidal cross-current stimulus with frequency $f + 1f$ was applied between the left temporal and occipital regions. (b) Change in SNR of $1f$ frequency component (from left to right, 10*Hz*, 20*Hz*, and 40*Hz*) before and after skull modification under the three stimulus combinations. The blue box shows the result before modification, and the red box shows the result after modification. (c) In dB, the topographic distribution of the SNR improvement of $1f$ frequency component (from left to right, 10*Hz*, 20*Hz*, 40*Hz*) under the three stimulus combinations before and after modification. The modification points are marked with red boxes in the figure. The redder the color, the higher the improvement. (d) The signal's spectrogram was recorded at the central point of the parietal region under the three stimulus combinations. The blue line shows the result before modification, and the red line shows the result after modification. $1f$ frequency component values and locations are indicated in the figure. (e) Comparison between direct low-frequency stimulation ($1f$) and TI stimulation protocol. The green line illustrates the spectrogram of the signal recorded at the central potential electrode using direct low-frequency stimulation ($1f$), whereas the red line depicts the spectrogram of the signal recorded during the application of the TI stimulation protocol.

overlap with the frequency of the electrophysiological signals we measure, avoiding any interference between the stimulation and the recordings. By integrating these innovations, we have successfully achieved a real-time bi-directional BCI solution, enabling simultaneous recording and stimulation in an in vitro setting. This approach opens up promising avenues for further research and application in BCIs and brain science.

A. The Significance of Real-Time

Unlike previous studies focusing on post-stimulation effects, our protocol enables a simultaneous bi-directional BCI, allowing us to obtain EEG signals during tACS [33]. We observed some interesting experimental results that have rarely been reported during the recording process. The most notable of these is that the EEG recordings evoked by the TI protocol show significant peaks not only at the difference frequencies (Δf) but also at their multiples. For example, in Fig. 5d., there is a higher peak at $20Hz$ in the recordings with a Δf of $10Hz$ and a significant peak at $40Hz$ in the experiments with a Δf of $20Hz$. The underlying neural mechanism of this phenomenon is unknown, and it is unclear whether this is specific to TI or whether all tACS stimuli induce harmonics. Our bi-directional BCI scheme could be an essential tool for studying the physiological mechanisms of tACS in the future.

B. Application of Skull Modification in BCI

The skull modification, a pivotal component of our proposed scheme, acts as a "solid" spatial filter rather than a mere signal enhancer. This remarkable phenomenon is visually evident in Fig. 2b, where the method selectively enhances signals from local brain regions. This feature holds immense significance in BCI research, as most BCI tasks focus on specific brain regions [34]. For instance, the SSVEP paradigm targets the occipital regions [25], while motor imagery and handwriting recognition tasks concentrate on the parietal regions [35], [36].

The "solid" spatial filter attribute of the skull modification allows researchers to effectively eliminate interference from other brain regions, thus significantly improving the performance of the target task. As a result, the future of skull modification in the field of BCI looks promising, extending beyond studies limited to parietal and occipital regions to include BCI investigations in temporal and frontal regions. Nonetheless, it is essential to acknowledge that the efficacy of skull modification may be constrained for certain BCI tasks

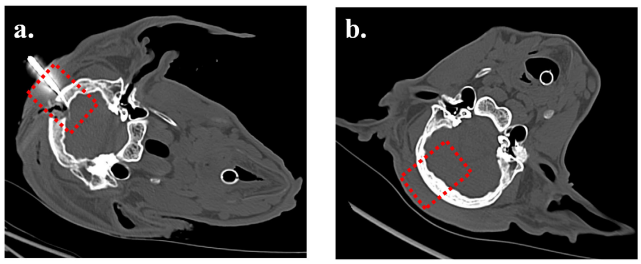

Fig. 6. illustrates the process of cranial healing. (a) displays the CT image immediately after the skull modification, while (b) presents the CT image taken one-month post-surgery. The red circle highlights the region on the skull where the modification was performed.

that target deeper brain regions, such as tactile and auditory processes, due to the associated risks and dangers of punching holes in the side or underneath the skull.

In conclusion, the development and application of skull modification in BCI research present valuable opportunities for enhancing brain signal analysis and fostering advances in neurotechnology. However, careful consideration of safety and appropriate utilization is necessary, particularly when dealing with tasks that involve deeper brain regions.

C. Security Considerations in Skull Modification

The use of ultrasound vibration to modify the skull entails certain risks that demand careful examination. To assess the extent of damage caused by skull modification, we conducted continuous CT monitoring on the sheep subjects involved in the experiment, as illustrated in Figure 6. The CT results revealed remarkably rapid healing of the sheep's modified skulls, with no discernible holes visible in the CT images within a month. This contrasts with previous findings in rats, where similar holes failed to heal in larger crania [20]. We attribute this difference to the disparity in cranial size, as sheep possess larger crania, which subjects them to more stress. Consequently, the holes can be sealed through deformation within a short timeframe, thereby expediting the healing process. Moreover, throughout the continuous monitoring, the sheep maintained good health.

Collectively, these findings lead us to conclude that the effects of skull modification on large mammals are minimal and reversible. Nevertheless, its practical application may be subject to individual variations and other factors. Therefore, conducting further clinical studies is imperative to validate the method's efficacy and safety, and to establish the optimal surgical protocol and parameter settings.

D. Comparison With Similar Technologies

Our work exhibits several advantages over traditional non-implantation electrical stimulation and recording. However, when compared to implantable technology, it does have some limitations in both recording and stimulation capabilities. For instance, a study revealed that the enhancement of SSVEP over EEG on ECoG can reach 7 dB and above [37], whereas our protocol achieves a maximum of only 5 dB. Furthermore, our enhancement of effective bandwidth for rsEEG falls short compared to implantable techniques such as stentrode [38].

Regarding stimulation, the accuracy of the TI scheme is influenced by the precision of the electric field and is not as proficient as techniques found in implantable DBS [19], [39]. Nevertheless, a significant advantage of our approach is the elimination of the need for electrode implantation, thereby mitigating numerous risks related to biocompatibility and ethics. We firmly believe that our scheme has the potential to partially replace implantable devices in the future, particularly in medical scenarios where exceptional precision is not a strict requirement.

V. Conclusion

Our solution presents a secure and convenient alternative to traditional invasive BCI technologies. The surgical procedure utilized in our approach is minimally invasive, involving a cranial opening diameter of only $500\mu m$, and the experimental cranial modification can be completed within a rapid 30 seconds. Notably, our solution does not require sensor implantation, thus mitigating the risks associated with biocompatibility. Moreover, in comparison to conventional non-implantation techniques, our solution offers superior signal quality and bandwidth for electrophysiological recording, potentially surpassing the performance limitations of current non-implantation BCIs.

The local impedance reduction resulting from the skull modification enables us to conduct TI protocols in vitro, thereby facilitating simultaneous electrical stimulation and electrophysiological recording. This groundbreaking feature opens up avenues for studying diseases and neural recordings, as well as future bi-directional closed-loop BCI investigations.

Acknowledgment

The authors would like to thank Ziyu Zhang from Xiamen University and Yuqing Zhao from the Central Academy of Fine Arts for their help in drawing the pictures in this article.

Competing Interests

The authors declare no competing interests.

References

[1] J. R. Wolpaw et al., "Brain–computer interface technology: A review of the first international meeting," *IEEE Trans. Rehabil. Eng.*, vol. 8, no. 2, pp. 73–164, Jun. 2000, doi: 10.1109/TRE.2000.847807.

[2] X. Gao, Y. Wang, X. Chen, and S. Gao, "Interface, interaction, and intelligence in generalized brain–computer interfaces," *Trends Cogn. Sci.*, vol. 25, no. 8, pp. 671–684, Aug. 2021, doi: 10.1016/j.tics.2021.04.003.

[3] C. Hughes, A. Herrera, R. Gaunt, and J. Collinger, "Bidirectional brain–computer interfaces," in *Handbook of Clinical Neurology*, vol. 168. Amsterdam, The Netherlands: Elsevier, 2020, pp. 163–181, doi: 10.1016/B978-0-444-63934-9.00013-5.

[4] A. G. Rouse et al., "A chronic generalized bi-directional brain–machine interface," *J. Neural Eng.*, vol. 8, no. 3, Jun. 2011, Art. no. 036018, doi: 10.1088/1741-2560/8/3/036018.

[5] W. J. Sohn et al., "Benchtop and bedside validation of a low-cost programmable cortical stimulator in a testbed for bi-directional brain–computer-interface research," *Frontiers Neurosci.*, vol. 16, Jan. 2023, Art. no. 1075971, doi: 10.3389/fnins.2022.1075971.

[6] W. J. Sohn et al., "A prototype of a fully-implantable charge-balanced artificial sensory stimulator for bi-directional brain–computer-interface (BD-BCI)," in *Proc. 42nd Annu. Int. Conf. IEEE Eng. Med. Biol. Soc. (EMBC)*, Jul. 2020, pp. 3083–3085, doi: 10.1109/EMBC44109.2020.9176718.

[7] S. Ryun, Y. J. Yang, J. Kwon, J. S. Kim, and C. K. Chung, "Macroscopic aspects of bi-directional BCI in human," in *Proc. 8th Int. Winter Conf. Brain-Comput. Interface (BCI)*, Feb. 2020, pp. 1–4, doi: 10.1109/BCI48061.2020.9061620.

[8] J. Herron, S. Stanslaski, T. Chouinard, R. Corey, T. Denison, and H. Orser, "Bi-directional brain interfacing instrumentation," in *Proc. IEEE Int. Instrum. Meas. Technol. Conf. (I2MTC)*, May 2018, pp. 1–6, doi: 10.1109/I2MTC.2018.8409795.

[9] L. Pycroft et al., "Brainjacking: Implant security issues in invasive neuromodulation," *World Neurosurg.*, vol. 92, pp. 454–462, Aug. 2016, doi: 10.1016/j.wneu.2016.05.010.

[10] V. S. Polikov, P. A. Tresco, and W. M. Reichert, "Response of brain tissue to chronically implanted neural electrodes," *J. Neurosci. Methods*, vol. 148, no. 1, pp. 1–18, Oct. 2005, doi: 10.1016/j.jneumeth.2005.08.015.

[11] H. Zhao, R. Liu, H. Zhang, P. Cao, Z. Liu, and Y. Li, "Research progress on the flexibility of an implantable neural microelectrode," *Micromachines*, vol. 13, no. 3, p. 386, Feb. 2022, doi: 10.3390/mi13030386.

[12] M. J. Vansteensel et al., "Towards clinical application of implantable brain–computer interfaces for people with late-stage ALS: Medical and ethical considerations," *J. Neurol.*, vol. 270, no. 3, pp. 1323–1336, Mar. 2023, doi: 10.1007/s00415-022-11464-6.

[13] J. Shi and Y. Fang, "Flexible and implantable microelectrodes for chronically stable neural interfaces," *Adv. Mater.*, vol. 31, no. 45, Nov. 2019, Art. no. 1804895, doi: 10.1002/adma.201804895.

[14] F. Frohlich, K. K. Sellers, and A. L. Cordle, "Targeting the neurophysiology of cognitive systems with transcranial alternating current stimulation," *Expert Rev. Neurotherapeutics*, vol. 15, no. 2, pp. 67–145, Feb. 2015, doi: 10.1586/14737175.2015.992782.

[15] J. M. Weiss, S. N. Flesher, R. Franklin, J. L. Collinger, and R. A. Gaunt, "Artifact-free recordings in human bidirectional brain–computer interfaces," *J. Neural Eng.*, vol. 16, no. 1, Feb. 2019, Art. no. 016002, doi: 10.1088/1741-2552/aae748.

[16] F. H. Kasten and C. S. Herrmann, "Recovering brain dynamics during concurrent tACS-M/EEG: An overview of analysis approaches and their methodological and interpretational pitfalls," *Brain Topography*, vol. 32, no. 6, pp. 1013–1019, Nov. 2019, doi: 10.1007/s10548-019-00727-7.

[17] N. Grossman et al., "Noninvasive deep brain stimulation via temporally interfering electric fields," *Cell*, vol. 169, no. 6, pp. 1029–1041.e16, Jun. 2017, doi: 10.1016/j.cell.2017.05.024.

[18] J. A. Malmivuo and V. E. Suihko, "Effect of skull resistivity on the spatial resolutions of EEG and MEG," *IEEE Trans. Biomed. Eng.*, vol. 51, no. 7, pp. 80–1276, Jul. 2004, doi: 10.1109/TBME.2004.827255.

[19] W. Guo et al., "A novel non-invasive brain stimulation technique: 'Temporally interfering electrical stimulation,"' *Frontries Neurosci.*, vol. 17, Jan. 2023, Art. no. 1092539.

[20] Y. Sun et al., "Minimally invasive local-skull electrophysiological modification with piezoelectric drill," *IEEE Trans. Neural Syst. Rehabil. Eng.*, vol. 30, pp. 2042–2051, 2022, doi: 10.1109/TNSRE.2022.3192543.

[21] F.-B. Vialatte, M. Maurice, J. Dauwels, and A. Cichocki, "Steady-state visually evoked potentials: Focus on essential paradigms and future perspectives," *Prog. Neurobiol.*, vol. 90, no. 4, pp. 418–438, Apr. 2010, doi: 10.1016/j.pneurobio.2009.11.005.

[22] G. Cruccu et al., "Recommendations for the clinical use of somatosensory-evoked potentials," *Clin. Neurophysiol.*, vol. 119, no. 8, pp. 1705–1719, Aug. 2008, doi: 10.1016/j.clinph.2008.03.016.

[23] B. Kotrikova et al., "Piezosurgery—A new safe technique in cranial osteoplasty?" *Int. J. Oral. Maxillofac. Surg.*, vol. 35, no. 5, pp. 461–465, May 2006, doi: 10.1016/j.ijom.2005.12.006.

[24] X. Chen, Y. Wang, M. Nakanishi, X. Gao, T.-P. Jung, and S. Gao, "High-speed spelling with a noninvasive brain–computer interface," *Proc. Nat. Acad. Sci. USA*, vol. 112, no. 44, Nov. 2015, doi: 10.1073/pnas.1508080112.

[25] X. Chen, Z. Chen, S. Gao, and X. Gao, "A high-ITR SSVEP-based BCI speller," *Brain-Computer Interface*, vol. 1, nos. 3–4, pp. 181–191, Oct. 2014, doi: 10.1080/2326263x.2014.944469.

[26] J. Mari-Acevedo, K. Yelvington, and W. O. Tatum, "Normal EEG variants," in *Handbook of Clinical Neurology*, vol. 160. Amsterdam, The Netherlands: Elsevier, 2019, pp. 143–160, doi: 10.1016/B978-0-444-64032-1.00009-6.

[27] D. H. Brainard, "The psychophysics toolbox," *Spatial Vis.*, vol. 10, no. 4, pp. 433–436, 1997, doi: 10.1163/156856897x00357.

[28] C. Cross et al., "International Organisation of Societies for Electrophysiological Technology (OSET): Guidelines for performing EEG and evoked potential monitoring during surgery," *Amer. J. Electroneurodiagnostic Technol.*, vol. 39, no. 4, pp. 257–277, Dec. 1999, doi: 10.1080/1086508x.1999.11079270.

[29] X. Chen, Y. Wang, S. Gao, T.-P. Jung, and X. Gao, "Filter bank canonical correlation analysis for implementing a high-speed SSVEP-based brain–computer interface," *J. Neural Eng.*, vol. 12, no. 4, Aug. 2015, Art. no. 046008, doi: 10.1088/1741-2560/12/4/046008.

[30] Y. Sun et al., "A binocular vision SSVEP brain–computer interface paradigm for dual-frequency modulation," *IEEE Trans. Biomed. Eng.*, vol. 70, no. 4, pp. 1172–1181, Apr. 2023, doi: 10.1109/TBME.2022.3212192.

[31] J. Thielen, P. van den Broek, J. Farquhar, and P. Desain, "Broadband visually evoked potentials: Re(con)volution in brain–computer interfacing," *PLoS ONE*, vol. 10, no. 7, Jul. 2015, Art. no. e0133797, doi: 10.1371/journal.pone.0133797.

[32] D. T. Bundy et al., "Characterization of the effects of the human dura on macro- and micro-electrocorticographic recordings," *J. Neural Eng.*, vol. 11, no. 1, Feb. 2014, Art. no. 016006, doi: 10.1088/1741-2560/11/1/016006.

[33] H. Matsumoto and Y. Ugawa, "Adverse events of tDCS and tACS: A review," *Clin. Neurophysiol. Pract.*, vol. 2, pp. 19–25, 2017, doi: 10.1016/j.cnp.2016.12.003.

[34] R. Abiri, S. Borhani, E. W. Sellers, Y. Jiang, and X. Zhao, "A comprehensive review of EEG-based brain–computer interface paradigms," *J. Neural Eng.*, vol. 16, no. 1, Feb. 2019, Art. no. 011001, doi: 10.1088/1741-2552/aaf12e.

[35] D. Zhang, K. Chen, D. Jian, and L. Yao, "Motor imagery classification via temporal attention cues of graph embedded EEG signals," *IEEE J. Biomed. Health Informat.*, vol. 24, no. 9, pp. 2570–2579, Sep. 2020, doi: 10.1109/JBHI.2020.2967128.

[36] F. R. Willett, D. T. Avansino, L. R. Hochberg, J. M. Henderson, and K. V. Shenoy, "High-performance brain-to-text communication via handwriting," *Nature*, vol. 593, no. 7858, pp. 249–254, May 2021, doi: 10.1038/s41586-021-03506-2.

[37] B. Wittevrongel et al., "Decoding steady-state visual evoked potentials from electrocorticography," *Frontiers Neuroinform.*, vol. 12, p. 65, Sep. 2018, doi: 10.3389/fninf.2018.00065.

[38] T. J. Oxley et al., "Minimally invasive endovascular stent-electrode array for high-fidelity, chronic recordings of cortical neural activity," *Nature Biotechnol.*, vol. 34, no. 3, pp. 320–327, Mar. 2016, doi: 10.1038/nbt.3428.

[39] Y. Chen et al., "Progress in the development of a fully implantable brain–computer interface: The potential of sensing-enabled neurostimulators," *Nat. Sci. Rev.*, vol. 9, no. 10, Sep. 2022, doi: 10.1093/nsr/nwac099.